J. Fluid Mech. (1978), *vol.* 86, *part* 4, *pp.* 705–726
Printed in Great Britain

Fluid transport by cilia between parallel plates

By N. LIRON

Department of Applied Mathematics, The Weizmann Institute of Science, Rehovot, Israel

(Received 8 September 1977)

The problem of fluid transport by cilia is investigated using the Green's function for a Stokeslet between two parallel plates. The discrete-cilia approach is used in building the model, and a readily usable expression for the velocities is obtained. Dependence on the direction of the metachronal wave and on time is not averaged out. Velocity fields, pressure fields and fluxes due to a single Stokeslet and to an infinite line of Stokeslets are discussed. It is found that the flux associated with Stokeslets in between two parallel plates is always zero, in contrast to a Stokeslet parallel to, and above, one plate. In the model one also has to add a plane Poiseuille flow, which incorporates non-zero flux. The flow due to the Stokeslet solution imposes a positive pressure gradient downstream, and the Poiseuille flow a negative pressure gradient. Calculated velocity profiles, in the pumping range, are seen to be time-independent in the centre of the channel and vary between a negative parabolic profile and a plug flow. The reason for these profiles and some possible biological applications are discussed.

1. Introduction

In an earlier paper (Liron & Mochon 1976*b*, henceforth referred to as LM) we dealt with the propulsion of an organism by cilia. The organism was treated as a flat plate in an infinite Newtonian fluid with a regular array of cilia beating in a metachronal fashion. A readily calculable expression for the velocity was obtained, enabling us to fit kinematically to observed beats, to derive velocity profiles, etc.

Another very important function that cilia perform is fluid transport, for such tasks as feeding and respiration in plants, or transport of gametes in the reproductive system. Lardner & Shack (1972) calculated flow of sperm in the ductus efferentes of the male reproductive tract, using an envelope model, and got results 50 times smaller than those observed (see also Blum 1974). Recognizing the need for a discrete-cilia model, Blake (1973) proposed using the model he developed for cilia above a flat plate in infinite fluid (Blake 1972), approximating a tubule by two parallel plates, taking the one-plate solution near each plate, and finally connecting the two profiles by a flat or parabolic profile (see also Blake & Sleigh 1974). Instead, it is suggested that one has to determine the solution for a Stokeslet in a confined region, and then to use that solution in the appropriate region. Also, the function of Stokeslets as fluid transporters should be looked into. The complete solution for a Stokeslet between two parallel plates was given by Liron & Mochon (1976*a*), and we apply it here to fluid transport.

The model we use is an infinite number of cilia, whose bases are equally spaced on a flat plate, with all cilia on the same x_2 line beating completely synchronously and identically, see § 2. This yields a flow which is periodic in the x_2 direction. An infinite

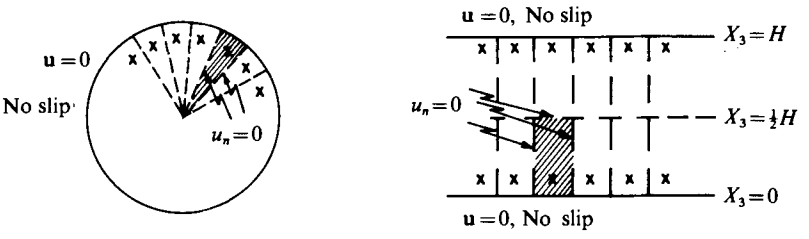

FIGURE 1. Similarity between pipe and channel for Stokeslet fields.

sequence of cilia lined identically on top and bottom plates at fixed x_2 are to be compared with a finite number of equally spaced cilia attached to the circumference of a tube, all the way around it. The similarity of flow in a pipe and channel can be seen in figure 1, where equal-strength Stokeslets are pointing into the paper at the crosses.

Each wedge in the pipe is periodically repeated, and on the wedge 'walls' we have the normal velocity equal to zero. This wedge (shaded area in pipe) is to be compared with a parallelepiped with the bottom wall at $x_3 = 0$, and the top 'wall' at $x_3 = \frac{1}{2}H$ (shaded area in channel). If Stokeslets are close to the wall and densely packed those two regions (wedge and parallelepiped) are very much alike. As Stokeslets get more and more dense, we approach an axisymmetric flow in the pipe, and a two-dimensional flow in the channel. Further similarities will be seen in §§3 and 4.

In §2 the model used is presented. This model is similar to the one in LM with the important exception that a plane Poiseuille flow has to be added here. Flux due to Stokeslets is discussed in §3, showing the basic difference between Stokeslets above one plate, and in between two plates. The first produces non-zero flux for a component parallel to the plate, but the latter always produces zero flux. Flow fields due to infinite lines and arrays of Stokeslets, their flux and pressure fields, are discussed in §4, and some numerical results given. The pressure field is discussed in §5. Numerical results for the model are given in §7. Ramifications of these results are discussed in §8.

2. The model, arrays of cilia

2.1. *One plane lined*

Let the plane on which the bases of the cilia are lined in a two-dimensional regular array be at $x_3 = 0$. The cilia array is depicted in figure 2. The co-ordinates of the centre-line of the cilium at the origin are

$$\boldsymbol{\xi}(s,t) = (\xi_1(s,t), \xi_2(s,t), \xi_3(s,t)), \quad 0 \leqslant s \leqslant L, \quad 0 \leqslant t \leqslant T, \tag{2.1}$$

where T is the period and L is the length of a cilium. All cilia are described in an array and their co-ordinates are

$$\boldsymbol{\xi}'_{m,n}(s,t) = (ma + \xi_1(s,\tau_m), nb + \xi_2(s,\tau_m), \xi_3(s,\tau_m)),$$
$$\tau_m = \kappa ma \pm \sigma t, \quad m,n = 0, \pm 1, \pm 2, \ldots. \tag{2.2}$$

This representation describes a metachronal wave in the x_1 direction, symplectic (minus sign in τ_m) or antiplectic (plus sign in τ_m). The wave has velocity $c = \sigma/\kappa$, wavelength $2\pi/\kappa$ and frequency $\sigma/2\pi$. The period is $T = 2\pi/\sigma$.

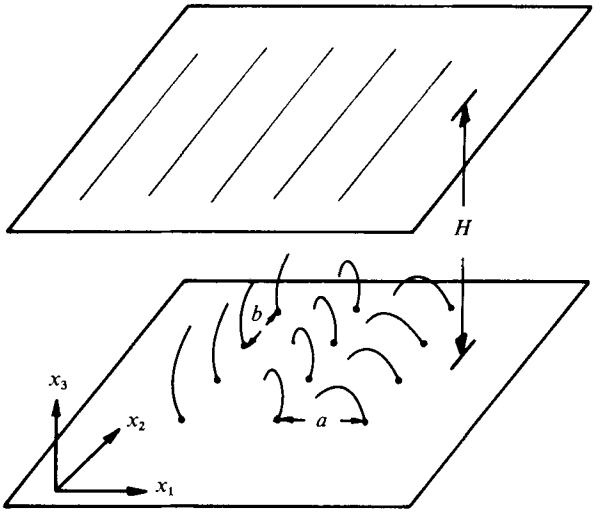

FIGURE 2. The model of cilia distribution.

The problem of a ciliated organism swimming in an infinite medium, which was approximated by an infinite plate with cilia attached to it, was treated in LM. Each cilium was approximated by a Stokeslet distribution along its centre-line. The basic Stokeslet solution was the solution for a Stokeslet above a flat plate (Blake 1971). The total velocity was found by summing over all cilia. The situation is somewhat different here, as one can add a plane Poiseuille flow to that found by summing over all cilia. The total velocity $\mathbf{u}$ between the two plates is composed of two parts,

$$\mathbf{u} = \mathbf{u}^{(1)} + \mathbf{u}^{(2)}, \tag{2.3}$$

where $\mathbf{u}^{(1)}$ is a plane Poiseuille flow in the x_1 direction, i.e.

$$u_j^{(1)}(\mathbf{x}, t) = -\frac{1}{2\mu}\frac{\partial p^{(1)}}{\partial x_1} x_3(H - x_3)\,\delta_{j1}, \quad j = 1, 2, 3, \tag{2.4}$$

with

$$\frac{\partial p^{(1)}}{\partial x_1} = C(t). \tag{2.5}$$

We shall see later on that we can take $C(t)$ to be independent of t in the model.

The velocity field $\mathbf{u}^{(2)}$ is due to the Stokeslet distribution on all cilia, and is

$$u_j^{(2)}(\mathbf{x}, t) = \sum_{n=-\infty}^{\infty} \sum_{m=-\infty}^{\infty} \int_0^L F_k(\boldsymbol{\xi}'_{m,n}(s,t))\, G_j^k(\mathbf{x}, \boldsymbol{\xi}'_{m,n}(s,t))\, ds, \quad j = 1, 2, 3. \tag{2.6}$$

Here, each cilium is approximated by a distribution of Stokeslets of strength $\mathbf{F}$ along the centre-line. The basic Stokeslet solution (Green's function), $G_j^k(\mathbf{x}, \boldsymbol{\xi})$, is the jth component of velocity induced at $\mathbf{x}$ by a force singularity at $\boldsymbol{\xi}$ pointing in the k direction, with zero velocity on the planes $x_3 = 0$, $x_3 = H$ and $G_j^k \to 0$ as $x_1^2 + x_2^2 \to \infty$. This function is given by Liron & Mochon (1976*a*). As in LM, we assume the periodicity conditions

$$u_j(x_1, x_2, x_3, t) = u_j(x_1, x_2 + b, x_3, t), \tag{2.7}$$

$$u_j(x_1, x_2, x_3, t) = u_j(x_1 \pm a, x_2, x_3, t - \Delta t), \quad \Delta t = a\kappa/\sigma, \tag{2.8}$$

where the plus sign stands for antiplectic metachronism and the minus sign for symplectic metachronism. From (2.7) and (2.8) we deduce that

$$\mathbf{F}(\boldsymbol{\xi}'_{m,n}(s,t)) = \mathbf{F}(\boldsymbol{\xi}(s,\tau_m)), \tag{2.9}$$

where τ_m is defined in (2.2).

The proof is similar to that given in the appendix of LM, and hinges on the fact that the Green's function, in both cases, depends on x_1, ξ_1, x_2, ξ_2 only through $x_1-\xi_1$ and $x_2-\xi_2$. Taking an average in the x_2 direction we get

$$\bar{u}_j(x_1,x_3,t) = \frac{1}{b}\int_{-\infty}^{\infty} \sum_{m=-\infty}^{\infty}{}' \left\{\int_0^L F_k(\boldsymbol{\xi}^m)\, G_j^k(\mathbf{x},\boldsymbol{\xi}'_{m,0})\, ds\right\} dx_2 + u_j^{(1)}(\mathbf{x},t), \tag{2.10}$$

$$\boldsymbol{\xi}^m = \boldsymbol{\xi}(s,\tau_m), \quad j = 1,2,3,$$

and if we have for the wavelength

$$\lambda = m_0 a = 2\pi/\kappa, \tag{2.11}$$

that is we have m_0 different cilia configurations before the pattern repeats itself, then we obtain

$$\bar{u}_j(x_1,x_3,t) = \frac{1}{b}\sum_{r=0}^{m_0-1}\int_0^L F_k(\boldsymbol{\xi}^r)\, D_j^k(x_1-ra, x_3, \boldsymbol{\xi}^r(s,t))\, ds + u_j^{(1)}(\mathbf{x},t), \tag{2.12}$$

and the kernel D_j^k is

$$D_j^k(x,z,\boldsymbol{\xi}) = \int_{-\infty}^{\infty} \sum_{q=-\infty}^{\infty} G_j^k(x-qm_0a, x_2, z, \boldsymbol{\xi})\, dx_2. \tag{2.13}$$

This kernel can be brought into an amenable form for computational purposes using methods similar to those used in LM, see appendix. The pressure field associated with this flow field is discussed in § 5.

2.2. *Two planes lined*

Since we are interested in an approximation to a pipe we shall assume that both planes are lined with cilia in the same way, and the cilia lined on one plate have the same beat and the same wave speed as the cilia lined on the other plate. In other words we shall assume that the cilia whose bases are lined on the plate at $x_3 = H$ are a reflexion in the centre-plane $x_3 = \frac{1}{2}H$ of the cilia whose bases are on the plate at $x_3 = 0$. It is not essential that the cilia beat with the same phase on top and bottom plates. If each cilium has the same beat, and the wave speed is the same, then (2.9) still holds. The assumption of reflexion simplifies the computations. The reflexion conditions are

$$F_k(\xi_1,\xi_2,\xi_3) = (\delta_{k1}+\delta_{k2}-\delta_{k3})\, F_k(\xi_1,\xi_2,H-\xi_3), \tag{2.14}$$

and

$$D_j^k(x_1,x_3,\xi_1,\xi_2,H-\xi_3) = (\delta_{j\alpha}\delta_{k\beta}+\delta_{j3}\delta_{k3}-\delta_{j3}\delta_{k\alpha}-\delta_{k3}\delta_{j\alpha}) D_j^k(x_1,H-x_3,\xi_1,\xi_2,\xi_3)$$
$$\alpha = 1,2, \quad \beta = 1,2, \tag{2.15}$$

from which we get that the mean velocity in this case is

$$\bar{u}_j(x_1,x_3,t) = \frac{1}{b}\sum_{r=0}^{m_0-1}\int_0^L F_k(\boldsymbol{\xi}^r)\,[D_j^k(x_1-ra,x_3,\boldsymbol{\xi}^r(s,t))$$
$$+(\delta_{j1}+\delta_{j2}-\delta_{j3})\, D_j^k(x_1-ra,H-x_3,\boldsymbol{\xi}^r(s,t))\, ds + u_j^{(1)}(\mathbf{x},t), \quad j = 1,2,3. \tag{2.16}$$

For the definition of $\boldsymbol{\xi}^r$, see (2.10).

3. Flux and pressure due to Stokeslets

3.1. *Stokeslets above a flat plate*

The solution (Green's function) for the velocity due to a Stokeslet situated at $\boldsymbol{\xi} = (\xi_1, \xi_2, \xi_3)$ pointing in the kth direction ($k = 1, 2, 3$, Cartesian co-ordinates) was given by Blake (1971). This is

$$G_j^k(\mathbf{x}, \boldsymbol{\xi}) = \frac{1}{8\pi\mu}\left[\left\{\frac{\delta_{jk}}{r} + \frac{r_j r_k}{r^3}\right\} - \left\{\frac{\delta_{jk}}{R} + \frac{R_j R_k}{R^3}\right\},\right.$$
$$\left. + 2\xi_3(\delta_{k\alpha}\delta_{\alpha l} - \delta_{k3}\delta_{3l})\frac{\partial}{\partial R_l}\left\{\frac{\xi_3 R_j}{R^3} - \left(\frac{\delta_{j3}}{R} + \frac{R_j R_3}{R^3}\right)\right\}\right], \tag{3.1}$$

where

$$\alpha = 1, 2, \quad r = |\mathbf{r}|, \quad R = |\mathbf{R}|,$$

and

$$\mathbf{r} = (x_1 - \xi_1, x_2 - \xi_2, x_3 - \xi_3),$$
$$\mathbf{R} = (x_1 - \xi_1, x_2 - \xi_2, x_3 + \xi_3), \quad j = 1, 2, 3. \tag{3.2}$$

The flat plate is defined by $x_3 = 0$.

The pressure is given by

$$p^k = \frac{1}{4\pi}\left[\left(\frac{r_k}{r^3} - \frac{R_k}{R^3}\right) - 2\xi_3(\delta_{k\alpha}\delta_{\alpha l} - \delta_{k3}\delta_{l3})\frac{\partial}{\partial R_l}\left(\frac{R_3}{R^3}\right)\right]. \tag{3.3}$$

To find the total flux created by the Stokeslet in a given direction, we have to integrate G_j^k over a plane perpendicular to that direction. Clearly there is no net flux in the x_3 direction, since by incompressibility we can integrate over any plane perpendicular to the x_3 direction, so choose the plane $x_3 = 0$. Integrating we find that the total flux in a given direction is always zero except for the flux in the x_1 direction when the force singularity is also in that direction (or the x_2 direction with the force in x_2 direction). In this case we get

$$\int_{-\infty}^{\infty}\int_0^{\infty} G_1^1(\mathbf{x}, \boldsymbol{\xi})\, dx_3\, dx_2 = \int_{-\infty}^{\infty}\int_0^{\infty} G_2^2(\mathbf{x}, \boldsymbol{\xi})\, dx_3\, dx_1 = \frac{\xi_3}{\mu\pi}, \tag{3.4}$$

so that we get a net flux directly proportional to the height of the singularity above the plate. This result blends uniformly into the case of an infinite medium (no plate). As $\xi_3 \to \infty$ the total flux also tends to infinity. The solution for the velocity due to a Stokeslet in an infinite medium is

$$G_j^k(\mathbf{x}, \boldsymbol{\xi}) = \frac{1}{8\mu\pi}\left[\frac{\delta_{jk}}{r} + \frac{r_j r_k}{r^3}\right], \tag{3.5}$$

and clearly

$$\int_{-\infty}^{\infty}\int_{-\infty}^{\infty} G_1^1(\mathbf{x}, \boldsymbol{\xi})\, dx_2\, dx_3 = \infty.$$

From (3.3) we see that $p^k \to 0$, as $|r| \to \infty$, which is the same as for a Stokeslet in an infinite medium where the pressure is given by

$$p^k = \frac{1}{4\pi}\frac{r_k}{r^3}. \tag{3.6}$$

3.2. *Stokeslets between two flat plates*

The Green's function for a Stokeslet between two flat plates was given by Liron & Mochon (1976*a*). Because of the lengthy expressions we shall not reproduce them here, but rather the asymptotic form for large distances from the Stokeslet which suffices for our purposes. Let H be the distance between the two plates, and let x_i, ξ_i be measured in units of H. Then the Green's function is

$$G_j^k = -\frac{3}{2\pi\mu}\frac{1}{H}\xi_3(1-\xi_3)x_3(1-x_3)\frac{\partial}{\partial r_\beta}\left(\frac{r_\alpha}{\rho^2}\right)\delta_{j\alpha}\delta_{k\beta}$$

$$+\delta_{j\alpha}\delta_{k\beta}\left[O\left(\frac{r_\alpha}{\rho}\frac{r_\beta}{\rho}\rho^{-\frac{1}{2}}H^{-\frac{1}{2}}[\exp(-\rho y_1)+\exp(-\rho\pi)]\right)\right]$$

$$+\delta_{j3}\delta_{k3}O(\rho^{-\frac{1}{2}}H^{-\frac{1}{2}}\exp[-\rho y_1])+(\delta_{j3}\delta_{k\alpha}+\delta_{k3}\delta_{j\alpha})O\left(\frac{r_\alpha}{\rho}\rho^{-\frac{1}{2}}H^{-\frac{1}{2}}\exp[-\rho y_1]\right),$$

$$\rho^2 = r_1^2+r_2^2, \quad y_1 \simeq 4{\cdot}2124, \quad \rho \gg 1, \quad \alpha = 1,2, \quad \beta = 1,2. \tag{3.7}$$

$\mathbf{r}$ is given in (3.2) and α, β take on the values 1 and 2. Clearly the total flux in the x_3 direction is zero as before, without any computations. To get the flux in the x_1 direction (x_2 direction), we can take any x_1 (any x_2) because of incompressibility, thus we can take $\rho \gg 1$ and use (3.7). Integrating the exponential terms of G_1^1 over x_3 and x_2, one obtains finite numbers multiplying $\exp(-r_1 y_1)$ or $\exp(-r_1\pi)$ and, since r_1 is arbitrary, these terms have zero contributions to the total flux.

Also

$$\int_{-\infty}^{\infty}\frac{\partial}{\partial r_1}\left(\frac{r_1}{\rho^2}\right)dx_2 = -\int_{-\infty}^{\infty}\frac{\partial}{\partial r_2}\left(\frac{r_2}{\rho^2}\right)dx_2 = 0 \tag{3.8}$$

and it follows that the total flux is zero in all cases. This is clear since the far-field behaviour is (for a Stokeslet parallel to the plates) a two-dimensional source doublet in planes parallel to the two plates, with height-dependent strength, see Liron & Mochon (1976*a*). Clearly a source doublet induces zero flux in any given direction.

This result may be unexpected as it can be shown that the solution for a Stokeslet between two plates converges to the solution for a Stokeslet above one plate, if we let the other plate go to infinity keeping everything else fixed. Moreover, the convergence is uniform. Nevertheless the flux induced by a Stokeslet parallel to one plate is not zero in this direction whereas it is zero when a second plate is present, at any finite distance H.

The solution for the pressure for large distances from the Stokeslet is

$$p^k \sim \frac{3}{\pi H^2}\frac{r_\alpha}{\rho^2}\xi_3(1-\xi_3)\delta_{k\alpha}, \quad \alpha = 1,2, \tag{3.9}$$

where again r_α, ρ and ξ_3 are measured in units of H. Here we have the same type of exponentially small remainder terms as for the velocity given in (3.7), see Liron & Mochon (1976*a*). Again we see that $p^k \to 0$ as $\rho \to \infty$.

3.3. *Infinite sequence of Stokeslets*

The model we deal with considers a uniform infinite array of cilia, with all cilia whose bases are at $(x_1, bn, 0)$, $n = 0, \pm 1, \pm 2, \ldots$, beating synchronously. Thus one should look at a sequence of Stokeslets in between two plates, with co-ordinates

$$\boldsymbol{\xi}_n = (\xi_1, \xi_2 + nb, \xi_3), \quad n = 0, \pm 1, \pm 2, \ldots, \tag{3.10}$$

where $0 < \xi_3 < H$, and the two plates are at $x_3 = 0$ and $x_3 = H$. We assume these Stokeslets are all of equal strength and pointing in the x_1 direction. Clearly the total contribution from this sequence is a periodic velocity field in the x_2 direction with period b. Moreover their sum is a solution for the flow due to a Stokeslet at (ξ_1, ξ_2, ξ_3) pointing in the x_1 direction, inside a parallelepiped the walls of which are given by $x_3 = 0$, $x_3 = H$, $x_2 = \xi_2 + \frac{1}{2}b$, $x_2 = \xi_2 - \frac{1}{2}b$, with no-slip conditions on $x_3 = 0$, and $x_3 = H$, and zero normal velocity on $x_2 = \xi_2 \pm \frac{1}{2}b$. This parallelepiped repeats itself, see figure 1.

Summing for the flux, we get zero flux in each of the above parallelepipeds. Indeed if we have to solve for a Stokeslet inside a tube of arbitrary cross-section, then we also impose the condition that, as $x_1 \to \pm\infty$, $\mathbf{u} \to 0$. The flux is bounded by the maximum velocity multiplied by the cross-sectional area (which is finite) and since $\mathbf{u} \to 0$, we must have zero flux, by incompressibility, in general. By this argument we must have zero flux in each parallelepiped, and the solution there is given by the sum of the infinite sequence of the identical Stokeslets. By symmetry the contributions of all Stokeslets to the flux through one parallelepiped is equal to the contribution of one Stokeslet to the total flux between two plates, so the latter must be zero.

Thus, a basic difference between the Stokeslet in a partially confined region and in an 'open' region emerges. One should remember, though, that in the model we also have to add the plane Poiseuille flow $\mathbf{u}^{(1)}$, see (2.4).

If we sum the constributions for the pressure in the x_1 direction of the sequence of Stokeslets discussed above, see (3.10), when they are situated above one flat plate, then again the pressure goes to zero as $|r_1| \to \infty$. On the other hand if we sum the contributions to the pressure in the x_1 direction from the same sequence of Stokeslets situated between the plates, then the pressure does not go to zero as $|r_1| \to \infty$. Indeed, from (3.9), the pressure due to the above sequence is

$$\begin{aligned} p^1 &\sim \frac{3}{\pi H^2}\xi_3(1-\xi_3)\, r_1 \sum_{n=-\infty}^{\infty} \frac{1}{r_1^2 + (r_2 + nb)^2} \\ &= \frac{3}{\pi H^2}\xi_3(1-\xi_3)\, r_1 \frac{1}{b^2}\frac{\pi}{2(r_1/b)}\frac{\sinh(2\pi r_1/b)}{\sinh^2(\pi r_1/b) + \sin^2(\pi r_2/b)}, \\ &= \frac{3}{2H^2 b}\xi_3(1-\xi_3)\frac{\sinh(2\pi r_1/b)}{\sinh^2(\pi r_1/b) + \sin^2(\pi r_2/b)}, \end{aligned} \tag{3.11}$$

from which we get

$$\begin{aligned} p^1 &\to \frac{3}{H^2 b}\xi_3(1-\xi_3), \quad r_1 \to \infty; \\ p^1 &\to \frac{-3}{H^2 b}\xi_3(1-\xi_3), \quad r_1 \to -\infty. \end{aligned} \tag{3.12}$$

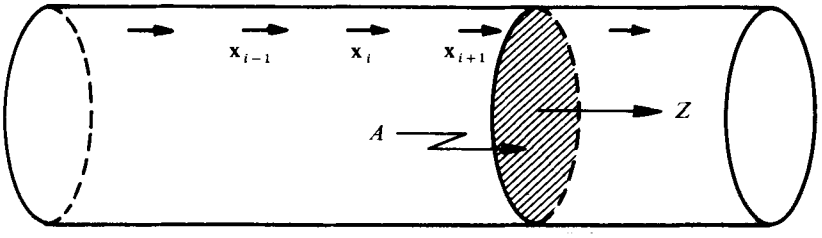

FIGURE 3. Infinite periodic sequence of Stokeslets down a pipe.

Thus this sequence of Stokeslets raises the pressure from a constant value $-A$ at $r_1 = -\infty$ to a value $+A$, at $r_1 = +\infty$, and the total pressure rise is $2A$. One should note again the parallelism between this result and the pressure due to a Stokeslet (or finite number of Stokeslets situated on a cross-section) in a pipe. If we have a Stokeslet in a pipe pointing in the z direction (see figure 3), then this Stokeslet will raise the pressure from some constant $-B$ at $z = -\infty$, to $+B$ at $z = +\infty$, Liron & Shahar (unpublished work).

4. Flow fields due to Stokeslets between two plates

Let us look at the pipe, or one parallelepiped of figure 1. To get the flux, one integrates the downstream velocity due to the contribution of all Stokeslets, over the pipe cross-section, plus the Poiseuille flow.

Let us look at an infinite periodic sequence of Stokeslets of unit strength all pointing downstream, as shown in figure 3. Let $u(\mathbf{x}, \mathbf{x}_i)$ be the velocity at a point $\mathbf{x}$ due to the Stokeslet at $\mathbf{x}_i$ in the z direction. The flux due to this line of Stokeslets is

$$Q = Q_1 + Q_2, \tag{4.1}$$

$$Q_1 = \iint_A \sum_{i=-\infty}^{\infty} u(\mathbf{x}, \mathbf{x}_i)\, dA,$$

A being the cross-section of the pipe. Q_1 is the flux due to the Stokeslet solutions, and Q_2 is the flux due to the Poiseuille flow. The flux due to each $\mathbf{x}_i$ separately is zero. The flux Q_1 will be zero if we can change the order of summation and integration (since A is compact, and all the functions $u(\mathbf{x}, \mathbf{x}_i)$ are continuous on A, for a cross-section not through one of the Stokeslets). This is permissible if the sum $\sum_{i=-\infty}^{\infty} u(\mathbf{x}, \mathbf{x}_i)$ is uniformly convergent for all $\mathbf{x}$ on A. The question is therefore, *how does the velocity* $u(\mathbf{x}, \boldsymbol{\zeta})$ *decay with distance* $\mathbf{x}$ *from the Stokeslet at* $\boldsymbol{\zeta}$. If the velocity decays like r^{-2} for instance (r measuring the distance), then convergence is uniform since we are summing a series of the form $\sum_n 1/n^2$. For a Stokeslet in an infinite medium velocity decays like r^{-1}, and we are not allowed to change the order of summation and integration.

As we shall see below the velocity field from the line of Stokeslets (3.10) decays exponentially up- or downstream (as is the case for a Stokeslet in a pipe), and thus

$$Q_1 = 0. \tag{4.2}$$

Let us consider again the infinite sequence of Stokeslets, all with the same strength, pointing in the kth direction, $k = 1$ or 2, and situated a distance b from each other as in §3.3. The Stokeslets' co-ordinates are as in (3.10),

$$\boldsymbol{\xi}_n = (\xi_1, \xi_2 + nb, \xi_3), \quad n = 0, \pm 1, \pm 2, \ldots, \tag{4.3}$$

and we want to find the velocity at the point $\mathbf{x} = (x_1, x_2, x_3)$. Let $\mathbf{r}$ be as in (3.2). Then, looking at $\mathbf{x}$ such that $\rho^2 = r_1^2 + r_2^2 \gg 1$, we get from (3.7) that

$$u_j^k(\mathbf{x}) \sim -\frac{3}{2\pi\mu}\frac{1}{H}\xi_3(1-\xi_3)x_3(1-x_3)\sum_{n=-\infty}^{\infty}\frac{\partial}{\partial r'_\beta}\left(\frac{r'_\alpha}{\rho'^2}\right)\delta_{j\alpha}\delta_{k\beta},$$

$$r'_1 = r_1, \quad r'_2 = r_2 - nb, \tag{4.4}$$

where α and β take on the values 1 and 2.

For u_1^1 we have the sum

$$\sum_{n=-\infty}^{\infty}\frac{1}{r_1^2 + (r^2 - nb)^2} = \frac{\pi}{2br_1}\frac{\sinh(2\pi r_1/b)}{\sinh^2(\pi r_1/b) + \sin^2(\pi r_2/b)}. \tag{4.5}$$

We thus obtain

$$u_1^1 \sim -\frac{3}{2\pi\mu}\frac{1}{H}\xi_3(1-\xi_3)x_3(1-x_3)\frac{\pi}{2b}\frac{\partial}{\partial r_1}\left[\frac{\sinh(2\pi r_1/b)}{\sinh^2(\pi r_1/b) + \sin^2(\pi r_2/b)}\right]. \tag{4.6}$$

Differentiating the expression within the square brackets we see that it behaves like $\exp[-2\pi r_1/b]$ for $r_1 \gg 1$, and therefore this term is exponentially decreasing. For u_2^1 we have the term

$$\frac{\partial}{\partial r_1}\left(\frac{r'_2}{r_1^2 + r_2'^2}\right) = \frac{\partial}{\partial r_1}\left[\frac{r_2 - nb}{r_1^2 + (r_2 - nb)^2}\right] = \frac{\partial}{\partial r_2}\left[\frac{r_1}{r_1^2 + (r_2 - nb)^2}\right], \tag{4.7}$$

and we therefore obtain

$$u_2^1 \sim -\frac{3}{2\pi\mu}\frac{1}{H}\xi_3(1-\xi_3)x_3(1-x_3)\frac{\pi}{2b}\frac{\partial}{\partial r_2}\left[\frac{\sinh(2\pi r_1/b)}{\sinh^2(\pi r_1/b) + \sin^2(\pi r_2/b)}\right], \tag{4.8}$$

and again the same conclusion follows. u_1^2 is asymptotic to the same expression as u_2^1, and u_2^2 to the negative of u_1^1. Thus such a distribution of Stokeslets along a line reduces their influence to the vicinity of the line itself, with exponentially decaying influence away from the line, whether they act in the direction of the line, perpendicular to it, or in any other direction. In particular the velocity decays exponentially, away from the Stokeslet in each parallelepiped described in §3.3.

Again the same parallelism holds between this line of Stokeslets and a single Stokeslet in a pipe, where velocities decay exponentially away from it with $|z|$, see Liron & Shahar (unpublished work).

As mentioned above we model each cilium by a Stokeslet distribution along its centre-lines, see §2, and the sequence of cilia whose bases are at $(ma, nb, 0)$, $n = 0, \pm 1, \pm 2, \ldots$, all beat identically and synchronously. They all have the same Stokeslet distribution at each instant in time. Therefore the above result shows that the effect of this row of cilia, as far as appreciable fluid movement is concerned, is limited to the vicinity of this cilia row (ignoring the Poiseuille flow). If fluid is to be continuously moved along the top of the cilia layer, perhaps carrying with it food

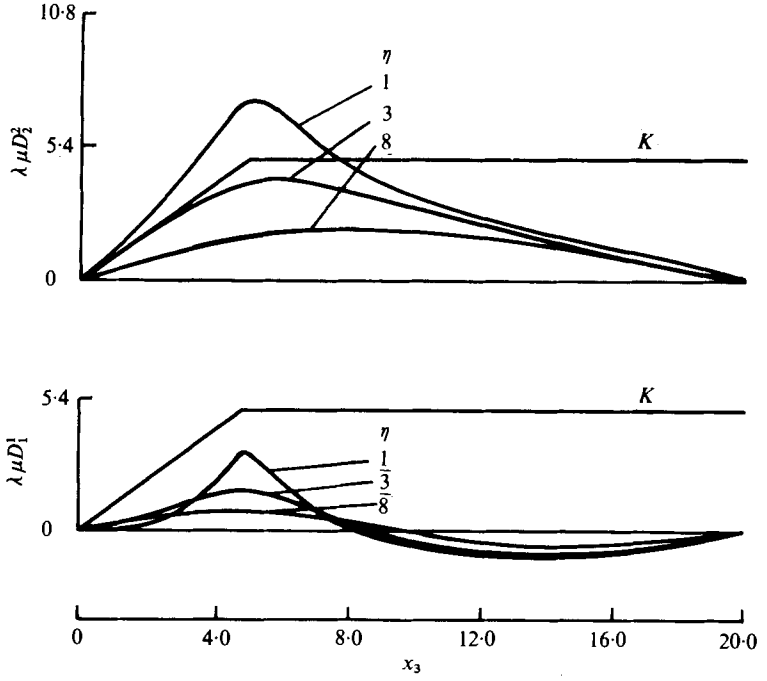

FIGURE 4. The kernels $\lambda\mu D_1^1$, $\lambda\mu D_2^2$, K *vs.* x_3 for various η, for $\kappa = 0{\cdot}3$, $\xi_3 = 5{\cdot}0$, $H = 20$. All quantities in μm. See (A 2).

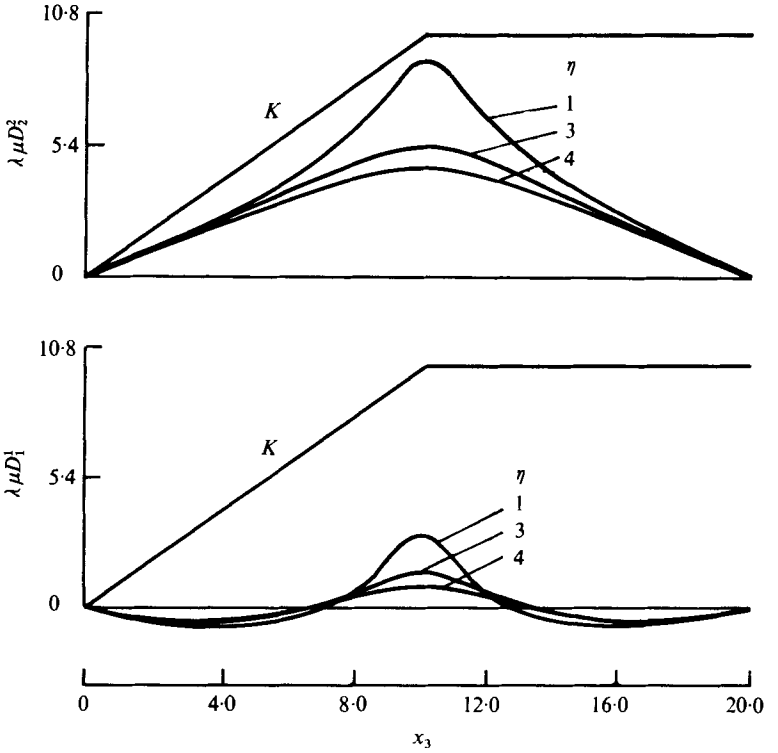

FIGURE 5. The kernels $\lambda\mu D_1^1$, $\lambda\mu D_2^2$, K *vs.* x_3 for various η, for $\kappa = 0{\cdot}3$, $\xi_3 = 10{\cdot}0$, $H = 20$. All quantities in μm. See (A 2).

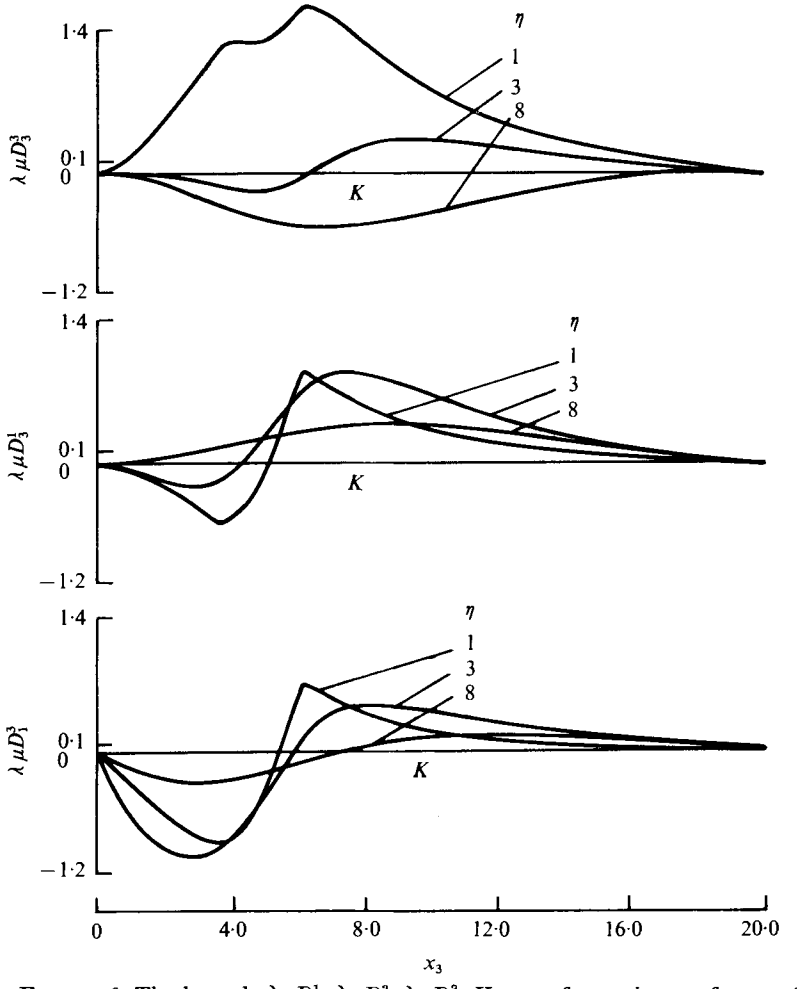

FIGURE 6. The kernels $\lambda\mu D_3^1$, $\lambda\mu D_1^3$, $\lambda\mu D_3^3$, K *vs.* x_3 for various η, for $\kappa = 0{\cdot}3$, $\xi_3 = 5{\cdot}0$, $H = 20$. All quantities in μm. See (A 3).

particles or some chemicals, then rows of cilia should be densely packed, densely enough that the near fields of adjacent rows overlap. This is indeed what is observed in ciliated organisms.

In the model we have lines of Stokeslets spaced at a distance a in the x_1 direction (up- and downstream). For $a \ll H$ (the biological situation), the far-field approximation is invalid, i.e. at no point are we far away from all lines of Stokeslets. Equation (4.6) does not depict the correct picture in this case. To demonstrate this let us look at equation (4.6), and integrate over r_2 (or x_2) over the width of one parallelepiped. We obtain zero flux [zero Q_1 in (4.1)] for any x_3, which is expected, since the dependence on x_3 is through $x_3(1-x_3)$ which is non-negative. That is, the flux is zero in each plane parallel to the walls (which is the picture of potentials). It follows that if, for some x_1 and x_3, we integrate the u_1^1 velocity along x_2 over the width of the parallelepiped, any appreciable deviations from zero would be due to the lines of Stokeslets near it (the contributions of the other lines are exponentially small anyway), and are therefore the near-field contribution.

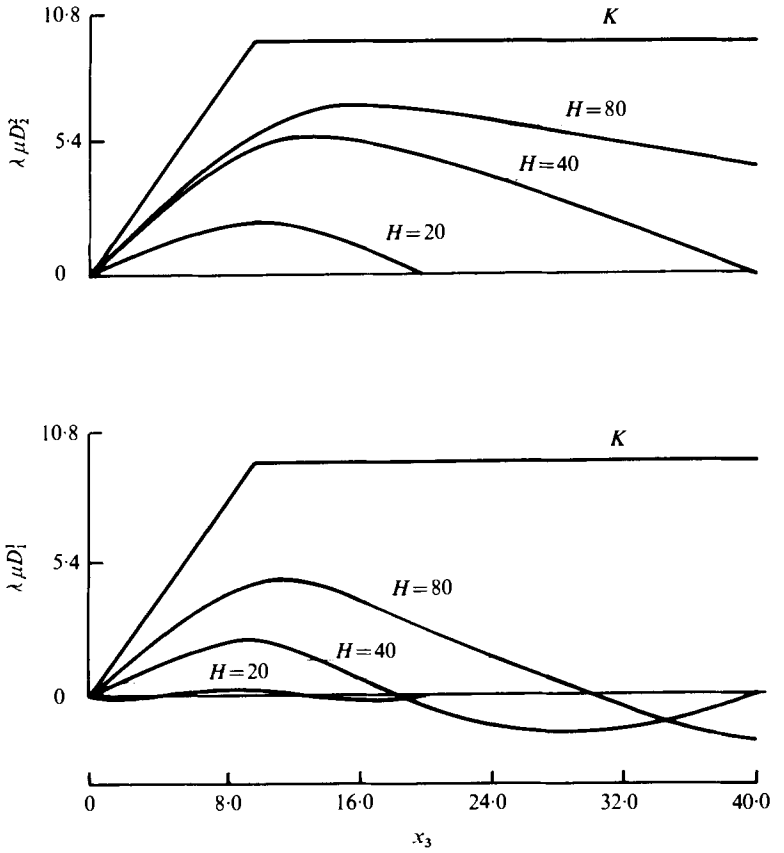

FIGURE 7. The kernels $\lambda\mu D_1^1$, $\lambda\mu D_2^2$, K *vs.* x_3 for various H, for $\kappa = 0{\cdot}3$, $\eta = 8{\cdot}0$, $\xi_3 = 9{\cdot}6$. All quantities in μm. See (A 2).

This suggested integral is exactly the kernel D_1^1 defined in equation (2.13) and given explicitly in the appendix.

The kernel $\lambda\mu D_j^k = (2\pi\mu/\kappa)\, D_j^k$ is given in figures 4 to 7 for various values of H, and compared with the kernel of Blake (1972), $K(x_3, \xi_3)$, see also LM. Figure 4 shows $\lambda\mu D_1^1$ and $\lambda\mu D_2^2$ *vs.* x_3, for $H = 20$, the Stokeslets situated at $\xi_3 = 5{\cdot}0$, for various values of $\eta = x_1 - \xi_1$. As in LM we take $\kappa = 0{\cdot}3$, and note that D_j^j blows up for $\eta = 0$ when $x_3 = \xi_3$, and that η is bounded by $\eta\kappa \leqslant \pi$.

Two results should be noted. The first is the large deviations of D_1^1, D_2^2 from K, much larger than the kernel H_j^k given in LM for the flow in a semi-infinite fluid above a flat plate. The second is that D_1^1 becomes negative on part of the x_3 axis. This is due to the fact that the total flux in the x_1 direction is zero. Since the kernel D_1^1 is the velocity of Stokeslets in the x_1 direction averaged over x_2, integrating over x_3 yields the flux of those Stokeslets in the x_1 direction and so must be zero. Consequently D_2^2 is closer to K than D_1^1. The same results can be seen for the symmetric case exhibited in figure 5, where $\xi_3 = 10$ and $H = 20$. For $\xi_3 = 5{\cdot}0$, $H = 20$, $\lambda\mu D_1^3$, $\lambda\mu D_3^1$ and $\lambda\mu D_3^3$ *vs.* x_3 are given in figure 6 (compared with the kernel $K \equiv 0$). Unlike the parallel one-plane case D_3^1 and D_1^3 are not so close as H_3^1 and H_1^3 (LM) and are given separately. These are certainly comparable to the 'major' terms D_1^1 and D_2^2. $\lambda\mu D_1^1$ and $\lambda\mu D_2^2$ for $\xi_3 = 9{\cdot}6$, $\eta = 8$, for

various H are shown in figure 7. As H increases, i.e. the second plate moves further and further away, D_1^1 and D_2^2 move closer to H_1^1 and H_2^2 respectively (and thus to K) given in LM, thus approaching the one-plane case for x_3 finite and fixed, and $H \to \infty$.

It should not be surprising that the kernel D_1^1 deviates from K. Flux exists in the one-plane case since the sum of the contributions of all Stokeslet solutions gives the complete flow picture. For the two-plate case the sum of all Stokeslet solutions does not give the complete flow picture and a Poiseuille flow has to be added. Thus K incorporates flux and, as we have seen, D does not.

5. The pressure field

Associated with the velocity field given in (2.12) we also have a pressure field. We have already seen that the infinite sequence of identical Stokeslets described in § 3.3 raises the pressure from $x_1 = -\infty$ to $x_1 = +\infty$ by a finite amount. Consequently it is not possible to sum the contributions to the pressure, but rather, one should look at the sum of contributions to the pressure gradient in the x_1 direction. Let the pressure field associated with $\mathbf{u}^{(1)}$ be $p^{(1)}$, $p^{(2)}$ associated with $\mathbf{u}^{(2)}$, and $p = p^{(1)} + p^{(2)}$. The average pressure gradient field (averaged over x_2) associated with the velocity field $\bar{u}$ given in (2.12) will be

$$\frac{\partial \bar{p}}{\partial x_1} = \frac{\partial \bar{p}^{(1)}}{\partial x_1} + \frac{\partial \bar{p}^{(2)}}{\partial x_1}, \tag{5.1}$$

where from (2.5)

$$\frac{\partial \bar{p}^{(1)}}{\partial x_1} = \frac{\partial p^{(1)}}{\partial x_1} = C(t), \tag{5.2}$$

and

$$\frac{\partial \bar{p}^{(2)}}{\partial x_1} = \frac{1}{b} \sum_{r=0}^{m_0-1} \int_0^L F_k(\boldsymbol{\xi}^r)\, B^k(x_1 - ra, x_3, \boldsymbol{\xi}^r(s,t))\, ds. \tag{5.3}$$

The kernel B^k is given by

$$B^k(x_1, x_3, \boldsymbol{\xi}) = \sum_{q=-\infty}^{\infty} \int_{-\infty}^{\infty} \frac{\partial p^k}{\partial x_1}(x_1 - qm_0 a, x_2, x_3, \boldsymbol{\xi})\, dx_2, \tag{5.4}$$

where p^k is the pressure field associated with the velocity field G_j^k discussed in § 2, and is given in Liron & Mochon (1976*a*).

Using methods similar to those in LM, one can transform the kernel B^k to the following form:

$$B^2 = 0,$$

$$\begin{aligned} B^k(x_1, x_3, \boldsymbol{\xi}) = \frac{\kappa}{\pi} \Bigg\{ & \delta_{k1} \sum_{q=1}^{\infty} \cos \eta\kappa q \left[\frac{\kappa q \sinh \xi_3 \kappa q \sinh (H - x_3)\kappa q}{\sinh H\kappa q} \right] \\ & - \delta_{k3} \sum_{q=1}^{\infty} \sin \eta\kappa q \left[\frac{\kappa q \sinh \xi_3 \kappa q \cosh (H - x_3)\kappa q}{\sinh H\kappa q} \right] \\ & + \sum_{q=1}^{\infty} [\cos \eta\kappa q A_5(\kappa q)\, \delta_{k1} - \sin \eta\kappa q A_6(\kappa q)\, \delta_{k3}] \Bigg\} \\ & + \frac{\kappa}{\pi} \frac{3}{H} \frac{\xi_3}{H} \left(1 - \frac{\xi_3}{H}\right) \delta_{k1}, \quad x_3 > \xi_3, \end{aligned} \tag{5.5}$$

where $\eta = x_1 - \xi_1$. For $x_3 < \xi_3$ replace x_3 by $H - x_3$, ξ_3 by $H - \xi_3$ and η by $-\eta$. The functions $A_5(\lambda)$, $A_6(\lambda)$ are (see Liron & Mochon 1976*a*)

$$A_5(\lambda) = \lambda^2[\sinh^2\lambda H - (\lambda H)^2]^{-1}$$
$$\times\left\{\left[\sinh\lambda H\frac{d}{d\lambda}\left(\frac{\sinh\lambda\xi_3}{\sinh\lambda H}\right)+\lambda H\frac{d}{d\lambda}\left(\frac{\sinh\lambda(H-\xi_3)}{\sinh\lambda H}\right)\right]\sinh\lambda H\sinh\lambda(H-x_3)\right.$$
$$\left.+[\lambda\xi_3 H\sinh\lambda(H-\xi_3)+(H-\xi_3)\sinh\lambda\xi_3\sinh\lambda H]\cosh\lambda(H-x_3)\right\},$$
$$A_6(\lambda) = \lambda^2[\sinh^2\lambda H - (\lambda H^2]^{-1}$$
$$\times\left\{[\lambda\xi_3 H\sinh\lambda(H-\xi_3)-(H-\xi_3)\sinh\lambda\xi_3\sinh\lambda H]\sinh\lambda(H-x_3)\right.$$
$$\left.-\left[\sinh\lambda H\frac{d}{d\lambda}\left(\frac{\sinh\lambda\xi_3}{\sinh\lambda H}\right)-\lambda H\frac{d}{d\lambda}\left(\frac{\sinh\lambda(H-\xi_3)}{\sinh\lambda H}\right)\right]\sinh\lambda H\cosh\lambda(H-x_3)\right\}. \quad (5.6)$$

The kernel $b^{-1}B^k$ gives the pressure gradient due to a doubly infinite sequence of Stokeslets of unit strength pointing in the kth direction, situated at

$$(\xi_1+n\lambda,\xi_2+mb,\xi_3), \quad n=0,\pm1,\ldots, \quad m=0,\pm1,\ldots, \quad \lambda=m_0a=2\pi/\kappa, \quad (5.7)$$

and averaged in the x_2 direction.

The average pressure rise per wavelength λ is, from (5.5),

$$\Delta\bar{p} = \frac{1}{b}\lambda\frac{\kappa}{\pi}\frac{3}{H}\frac{\xi_3}{H}\left(1-\frac{\xi_3}{H}\right)\delta_{k1} = \frac{6}{bH}\frac{\xi_3}{H}\left(1-\frac{\xi_3}{H}\right)\delta_{k1}. \quad (5.8)$$

Notice that this pressure rise is exactly the pressure rise from $-\infty$ to $+\infty$ due to the sequence of Stokeslets described in §3.3 [only $n=0$ in (5.7)] and given in (3.12). [The additional power of H in the denominator of (3.12) is due to the fact that b in (3.12) is measured in units of H, whereas we have not done this normalization here.] It follows from (5.3) that the pressure rise per wavelength for $\bar{u}_2$ is

$$\Delta\bar{p}^{(2)} = \frac{6}{bH}\sum_{r=0}^{m_0-1}\int_0^L F_1(\boldsymbol{\xi}^r)\frac{\xi_3^r}{H}\left(1-\frac{\xi_3^r}{H}\right)ds. \quad (5.9)$$

From (5.2) we obtain the pressure rise per wavelength due to the Poiseuille flow,

$$\Delta\bar{p}^{(1)} = \lambda C(t). \quad (5.10)$$

We are interested in the cilia performance in the pumping range. This range is the range for which we have non-negative average flux per period, $Q \geqslant 0$, while the pressure rise per wavelength is also non-negative, $\Delta p \geqslant 0$. It has been shown by Liron (1976) that for a periodic flow the pressure rise per wavelength is independent of the lateral co-ordinate x_3 at which it is measured. Although the flow field $\mathbf{u}^{(2)}$ in the sublayer region has large fluctuations, it turns out to be practically time independent (or equivalently independent of x_1), at about a height of $2L$, where L is the length of a cilium. This has been seen in LM and the reason for it will be explained below. Thus $\Delta\bar{p}^{(2)}$ is practically time independent. The flux is non-negative for $C(t) < 0$, since the contribution to the flux due to $\mathbf{u}^{(2)}$ is zero, see (4.2). We may therefore write

$$\Delta\bar{p} = (1-\alpha)\Delta\bar{p}^{(2)}, \quad (5.11)$$

where $0 \leqslant \alpha \leqslant 1$ in the pumping range, and $C(t) = C$ is a constant independent of time.

Let us look at the kernel D_1^1 given in the appendix. D_1^1 consists of a linear term in x_3, $(\kappa/2\pi\mu)\,\xi_3(1-x_3/H)$, a parabolic term in x_3, $(\kappa/2\pi\mu)\,3\xi_3(1-\xi_3/H)(1-x_3/H)\,x_3/H$, both independent of x_1, and several infinite series which do depend on x_1. If H is not too small then the infinite series can be neglected for x_3 not very close to ξ_3. A linear term does not have a pressure gradient associated with it. Thus, the dominant term in this region is the constant pressure gradient associated with the parabolic part. This is the constant term in (5.5) (which is independent of x_1 and x_3).

In the case of two planes lined, we have seen in §2.2 that we use the kernel $D_j^k(x_1, x_3, \boldsymbol{\xi}) + (\delta_{j1}+\delta_{j2}-\delta_{j3})\,D_j^k(x_1, H-x_3, \boldsymbol{\xi})$. In particular instead of D_1^1 we use $D_1^1(x_1, x_3, \boldsymbol{\xi}) + D_1^1(x_1, H-x_3, \boldsymbol{\xi})$. In this case the constant term in (5.5) is doubled, and likewise Δp changes to $2\Delta p$ in (5.8).

6. Integral equations for the force distribution

In order to find the force distribution on the cilia, to use in (2.12) or (2.16), we fit kinematically to an observed cilia beat, as has been done in LM. The averaging in the x_2 direction only is equivalent to replacing the discrete cilia by an array of waving sheets. We demand that, on all cilia, the computed velocity is the observed velocity. Thus for one plane lined,

$$\frac{\partial \xi_j^n(\bar{s})}{\partial t} = \bar{u}_j(\xi_1^n(\bar{s}) + na, \xi_3^n(\bar{s}), t)$$

$$= \frac{1}{b}\sum_{r=1}^{m_0-1}\int_0^L F_k[\boldsymbol{\xi}^r(s,t)]\,D_j^k[\xi_1^n(\bar{s}) + (n-r)\,a, \xi_3^n(\bar{s}), \boldsymbol{\xi}^r(s,t)]\,ds$$

$$+ u_j^{(1)}(\boldsymbol{\xi}(\bar{s}), t), \quad n = 0, 1, \ldots, m_0-1, \quad j = 1, 2, 3, \quad 0 \leqslant \bar{s} \leqslant L, \tag{6.1}$$

where $\boldsymbol{\xi}^r$ is defined in (2.10).

Equation (6.1) is not sufficient to determine the forces uniquely, as we have $\mathbf{u}^{(1)}$ at our disposal, see (2.4). Since we are interested in the pumping range, see §5, we may specify in addition either the flow rate Q, or the pressure rise per wavelength, $\Delta\bar{p}$ (which are proportional to one another). Choosing $\Delta\bar{p}$ as known, and combining (5.9) and (5.11) for the pressure rise, we obtain

$$\Delta\bar{p} = (1-\alpha)\frac{6}{bH}\sum_{r=0}^{m_0-1}\int_0^L F_1(\boldsymbol{\xi}^r(s))\,\frac{\xi_3^r(s)}{H}\left(1-\frac{\xi_3^r(s)}{H}\right)ds, \tag{6.2}$$

where α is a given number, $0 \leqslant \alpha \leqslant 1$.

The velocity $\mathbf{u}^{(1)}$ is then given by

$$u_j^{(1)} = \frac{1}{2\mu}\frac{\alpha}{1-\alpha}\frac{\Delta\bar{p}}{\lambda}x_3(H-x_3)\,\delta_{j1}. \tag{6.3}$$

The two extreme cases in the pumping range are as follows. (i) $Q = 0$, in this case $\alpha = 0$, $u^{(1)} \equiv 0$ and we are left to solve only (6.1). Here $\Delta\bar{p}$ is maximal. (ii) $\Delta\bar{p} = 0$. In this case $\alpha = 1$ and we get the maximum flux, $Q^{\max}$.

For all cases $0 \leqslant \alpha \leqslant 1$, we can combine (6.1), (6.2) and (6.3) into one equation.

Equations (6.1)–(6.3) are non-dimensionalized by taking L as the length scale, σL as the velocity scale, σ^{-1} as the time scale and $\mu\sigma L^2$ as the force scale (F_k in the equations is force per unit length and has dimensions of $\mu\sigma L$).

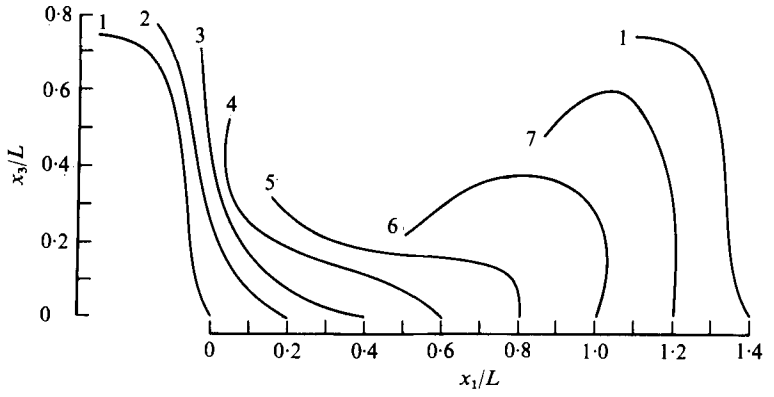

FIGURE 8. The model for cilia beat (reproduced by the computer) for one wavelength. Increasing numbers indicate positions of cilium in consecutive fixed time intervals. $\lambda/L = 1{\cdot}4$.

Equations (6.1)–(6.3) now become

$$\frac{\partial \xi_j^n}{\partial t}(\bar{s}) = \frac{1}{2\pi b}\sum_{r=0}^{m_0-1}\int_0^L F_k(\xi^n(s,t))\{2\pi\mu D_j^k[\xi_1^n(\bar{s})+(n-r)a, \xi_3^n(\bar{s}), \xi^r(s,t)]\}\,ds$$
$$+u_j^{(1)}(\xi(\bar{s},t)), \quad n=0,\ldots,m_0-1, \tag{6.4}$$

$$\Delta\bar{p} = (1-\alpha)\frac{6}{bH}\sum_{r=0}^{m_0-1}\int_0^1 F_1(\xi^r)\frac{\xi_3^r}{H}\left(1-\frac{\xi_3^r}{H}\right)ds, \tag{6.5}$$

$$u_j^{(1)} = \frac{x_3}{H}\left(1-\frac{x_3}{H}\right)(\tfrac{1}{2}H^2)\frac{\alpha}{1-\alpha}\frac{\Delta\bar{p}}{\lambda}\delta_{j1}. \tag{6.6}$$

Now all quantities are non-dimensional, i.e. b, a, λ, H, ξ stand for $b/L, a/L, \lambda/L, H/L, \xi/L$ respectively, etc. For two planes lined we again have (6.4)–(6.6), where we replace $D_j^k(x_1, x_3, \xi)$ by $D_j^k(x_1, x_3, \xi)+(\delta_{j1}+\delta_{j2}-\delta_{j3})\,D_j^k(x_1, H-x_3, \xi)$, and replace $\Delta\bar{p}$ by $2\Delta\bar{p}$.

These equations were solved numerically and the details are discussed in the next section.

7. Numerical results

7.1. *Description of the moving cilium and solution of integral equations*

The description of the moving cilium is achieved by discretizing it and fitting each segment by a Fourier series in time to the path of the corresponding section of the cilium. This method is described in LM. We use the same beat that we used in LM. In figure 8 we depict the different cilia in one wavelength, which correspond also to different positions of one cilium at fixed time intervals in one time period. Increasing numbers represent increasing time.

To solve for the forces in (6.4), (6.5) we replace the integrals by a quadrature formula (we used the mid-point rule), thus having to solve $3m_0N$ linear inhomogeneous equations with the same number of unknowns. It should be noted that, when doing this, singularities occur in D_j^k when $r = n$ and s is equal to one of the nodes of the quadrature formula. Since $D_j^k(\mathbf{x}, \xi)$ is the velocity at $\mathbf{x}$ due to a Stokeslest at ξ, and we want to match velocities on the cilium surface, we replace $D_j^k(\xi_1, \xi_3, \xi)$ by

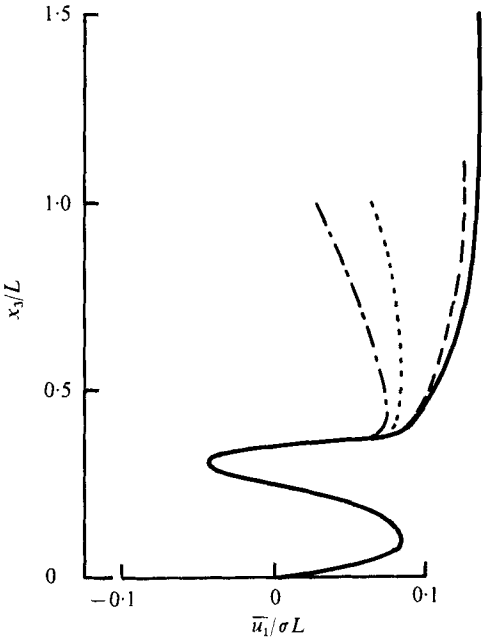

FIGURE 9. Velocity component in the x_1 direction, $\bar{u}_1(x_1, x_3)$, for $Q = 0$ in the cilia layer *vs.* x_3 for various values of H: ——, $H = \infty$; – – –, $H = 100L$, ···; $H = 10L$; – · – · –, $H = 10L$ with both planes lined with cilia. $x_1 = \lambda/4L$. Beat as in figure 8.

$D_j^k(\xi_1 + \delta, \xi_3, \boldsymbol{\xi})$ for those points, where δ is the cilium radius. This will yield a large, but finite, number.

We are interested in the pumping range, and as we have already pointed out in the previous section the case of $Q = 0$ yields the maximum $\Delta\bar{p}$. We therefore solve the equations in this range in two steps.

Step 1. Solve (6.2) with $\mathbf{u}^{(1)} = 0$, and then obtain $\Delta\bar{p}^{\max}$, from (6.5), taking $\alpha = 0$, there.

Step 2. Take $\Delta\bar{p} = (1-\alpha)\,\Delta\bar{p}^{\max}$ in (6.5), for some $0 < \alpha \leqslant 1$, and then solve (6.4)–(6.6), or equivalently solve

$$\frac{\partial \xi_j^n}{\partial t} - \alpha \frac{\xi_3^n}{H}\left(1 - \frac{\xi_3^n}{H}\right) \tfrac{1}{2} H^2 \frac{\Delta\bar{p}^{\max}}{\lambda} \delta_{j1} = \frac{1}{2\pi b} \sum_{r=0}^{m_0-1} \int_0^1 F_k(\boldsymbol{\xi}^r(s,t)) \{2\pi\mu D_j^k[\xi_1^n + (n-r)\,a, \xi_3^n, \boldsymbol{\xi}^r(s,t)]\}\, ds, \quad n = 0, 1, \ldots, m_0 - 1. \tag{7.1}$$

For the two planes lined with cilia, replace D_j^k and $\Delta p^{\max}$ appropriately, as described above.

7.2. *Velocity profiles*

We demonstrate the results by showing some calculated velocity profiles. In figure 9 velocity profiles in the cilia sublayer are shown for $x_1 = \lambda/4L$, for the case of $Q = 0$ ($\Delta\bar{p} = \Delta\bar{p}^{\max}$). We see that the presence of the top plate reduces the velocity at the top of the cilia layer, but that it approaches the velocity of the one-plane case as the distance between the plates increases.

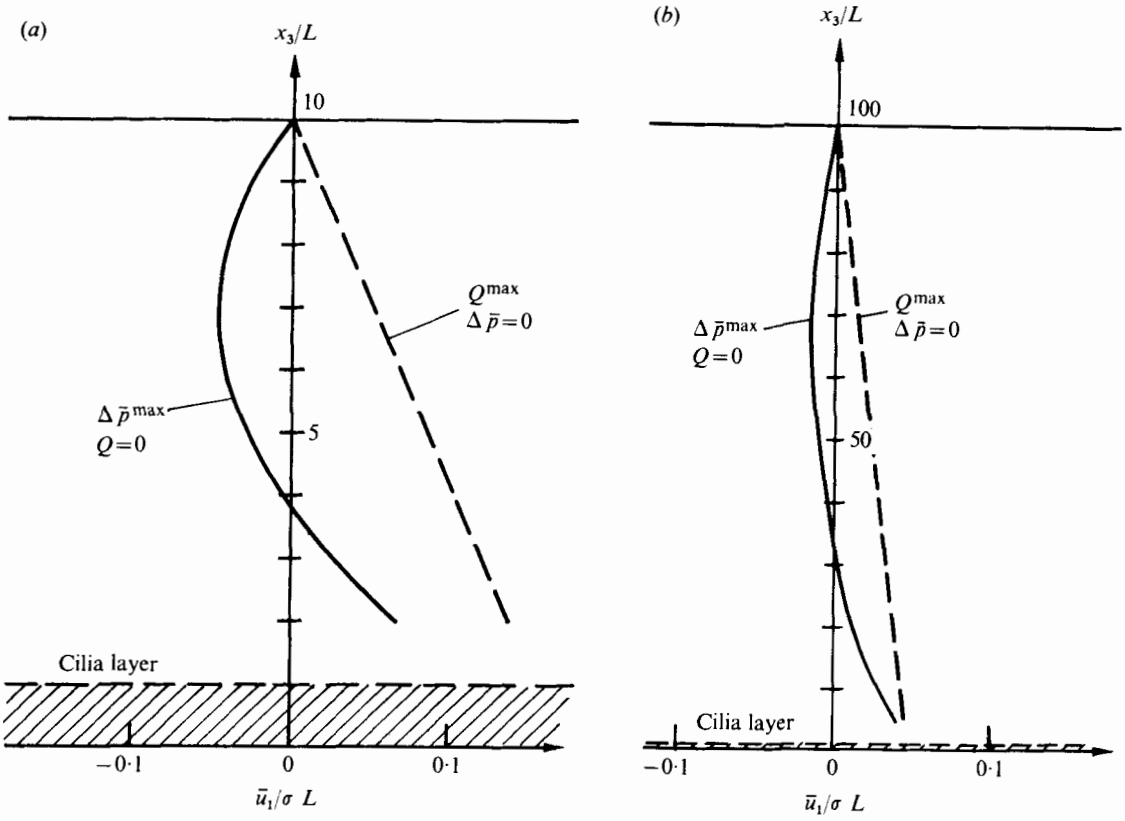

FIGURE 10. Velocity component in the x_1 direction, $\bar{u}_1(x_1, x_3)$, outside the cilia layer for $Q = 0$, and for $\Delta\bar{p} = 0$, one plane lined. (*a*) $H = 10L$, (*b*) $H = 100L$. Beat as in figure 8.

Two examples of velocity profiles in the region between the plates, outside the cilia layer(s), are shown in figures 10 and 11. The two cases shown are $H = 10L$ and $H = 100L$ for one plane lined in figures 10(*a*) and (*b*), and for two planes lined in figures 11(*a*) and (*b*). These profiles are independent of x_1 (or t) and in each the two extreme cases are shown; $Q = 0$, $\Delta\bar{p}^{max}$ and $\Delta\bar{p} = 0$, Q^{max}.

Of particular interest is the result that the profiles are time independent, and that for $\Delta\bar{p} = 0$ we get a flat velocity profile, i.e. a plug flow for two planes lined. Closer to the cilia layer(s) velocity profiles do exhibit time fluctuations but blend into the given profiles. These results are discussed in the next section.

8. Discussion

We have presented here a model of cilia fluid transport between parallel plates. The model for the cilia layer(s) depends both on time and on the direction of the metachronal wave. Similarities between this model and flow in a tube were shown, so that the same qualitative phenomena are expected to occur also in the tube. A Stokeslet above a flat plate was compared with a Stokeslet between flat plates. It was found that a Stokeslet above a flat plate creates a non-zero flux when pointing parallel to the plate, whereas a Stokeslet between parallel plates produces zero flux. Unlike the one-

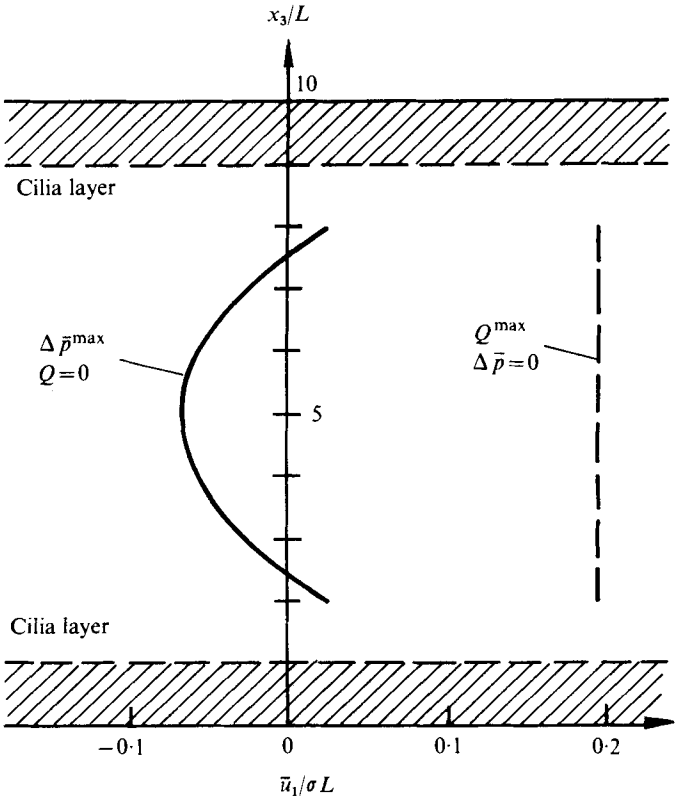

FIGURE 11 (*a*). For legend see next page.

plate case, where the solution is obtained by summing over all Stokeslets, in the two-plate case one must also add a plane Poiseuille flow. The Stokeslet solution alone creates a positive pressure rise per wavelength Δp, with zero flux ($Q = 0$). Lowering the pressure rise per wavelength causes a positive flux.

We are interested in the pumping range ($Q \geqslant 0$, $\Delta p \geqslant 0$), and velocity profiles for the two extreme cases are shown in figures 10 and 11 both for one plane lined and for two planes lined. In the mid-region between the plates the velocity profiles are time independent. The reason for this is the structure of D_1^1 given in the appendix, and is explained in §5.

For one plane lined D_1^1, which is the Stokeslet solution only, consists essentially of a linear function and a parabolic function in the mid-region. This explains the profiles for $Q = 0$, $\Delta\overline{p}^{\max}$, in figures 10(*a*) and (*b*). The other extreme in the pumping range is $\Delta\overline{p} = 0$, and is seen to be a linear function. Indeed, only the parabolic profile has a pressure gradient associated with it, and demanding that $\Delta p = 0$ is equivalent to the annihilation of the parabolic part in the $Q = 0$ profiles, leaving only the linear part.

The case $\Delta\overline{p} = 0$ is of particular interest for one plane lined, as this can be looked upon as a swimming ciliated organism next to a wall. This is achieved by moving the non-ciliated wall in order to create an opposite shear flow exactly cancelling the shear flow profile in figures 10(*a*) and (*b*) (the co-ordinate system is moving with the ciliated plate). The condition $\Delta\overline{p} = 0$ is equivalent to the demand that the average force per

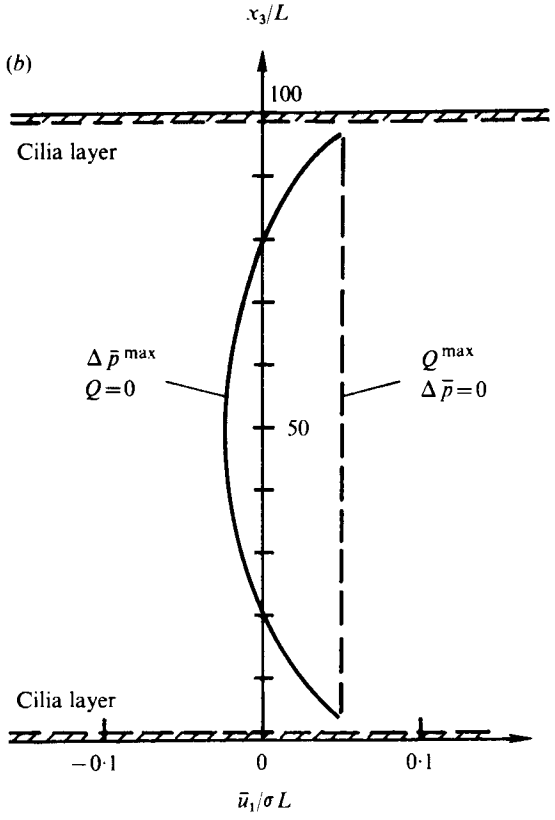

FIGURE 11. Velocity component in the x_1 direction, $\bar{u}_1(x_1, x_3)$, in the mid-region for $Q = 0$, and for $\Delta\bar{p} = 0$, two planes lined. (*a*) $H = 10L$, (*b*) $H = 100L$. Beat as in figure 8.

wavelength on the organism is zero. In the case of a swimming organism in infinite fluid, treated in LM, one can check that indeed $\Delta\bar{p} = 0$ there.

For two planes lined the kernel replacing D_1^1 is a combination of D_1^1 on both plates. In the mid-region it turns out to be essentially a parabolic profile, with twice the pressure gradient as in the previous case, and in addition this time, not a linear function, but a constant. This explains the parabolic profiles we see for $Q = 0$ in figures 11 (*a*) and (*b*). Again only the parabolic part has a pressure gradient associated with it, and thus for the case $\Delta\bar{p} = 0$ we are left with the constant part only. This explains the 'plug flow' we observe in figures 11 (*a*) and (*b*) for $\Delta\bar{p} = 0$. Blake (1973) has suggested using the one-plane model on each plate, and joining them by a flat profile. We see that this would indeed be a good approximation if the two plates are not too close (relative to a cilium length), and provided the additional condition, $\Delta\bar{p} = 0$, is met, i.e. the pumping by the cilia operates at 'peak performance'. As we see, in this case the cilia operate to provide a free slip condition near the boundaries, resulting in a plug flow in the middle region. If $\Delta\bar{p} > 0$, the profiles in the mid-region will lie between the two profiles given in figure 11.

Both the case $Q = 0$ and the case $Q > 0$ may be of biological importance. As seen in figure 11 (*a*), if cilia extend a non-negligible distance into the channel, the backflow is quite strong for $Q = 0$ in the middle region of the channel. This may explain the

ability of sperm to be moved up the oviduct from the uterus in the direction of the ovary (the ampulla–isthmus junction is completely occluded so that we must have $Q = 0$). This (rapid) movement is achieved although cilia beat in the direction of the uterus, and spermatozoa were observed to be swept along by the ciliary current when applied to the surfaces of opened oviducts at such a rate that their own flagellar activity was of almost no avail against the ciliary current, see Blandau (1969).

In the ductus efferentes of the male reproductive tract, water is known to be 'pushed' into the tubes across the membranes. Thus a positive flux is created. The velocity profiles may be a parabolic profile lying between the profiles depicted in figures 11 (*a*) and (*b*), or even a positive parabolic profile if the flux exceeds $Q^{\max}$ (and then $\Delta p < 0$).

This work was supported in part by the National Science Foundation (grant MCS 75-08328) while the author was Visiting Associate Professor at Rensselaer Polytechnic Institute.

Appendix

The kernel D_j^k given in (2.10) is

$$D_2^1 = D_1^2 = D_3^2 = D_2^3 = 0, \tag{A 1}$$

$$\begin{aligned}
D_j^j(x_1, x_3, \boldsymbol{\xi}) = \frac{\kappa}{2\pi\mu}\Big\{&(\delta_{j1}+\delta_{j2})\frac{\xi_3(H-x_3)}{H} \\
&+(1+\delta_{j2})\sum_{q=1}^{\infty}\cos\eta\kappa q\,\frac{\sinh\xi_3\kappa q\sinh(H-x_3)\kappa q}{\kappa q\sinh H\kappa q} \\
&+(\delta_{j1}-\delta_{j3})\sum_{q=1}^{\infty}\cos\eta\kappa q\,\frac{d}{dt}\left[\frac{\sinh\xi_3 t\sinh(H-x_3)t}{\sinh Ht}\right](t=\kappa q) \\
&-\delta_{j1}.3\xi_3(H-\xi_3)x_3(H-x_3)/H^3+(\delta_{j1}+\delta_{j3})\sum_{q=1}^{\infty}\kappa q\cos\eta\kappa q[x_3 H\cosh x_3\kappa q\sinh\xi_3\kappa q \\
&-x_3\xi_3\sinh H\kappa q\cosh(H-x_3-\xi_3)\kappa q+H\xi_3\sinh x_3\kappa q\cosh\xi_3\kappa q \\
&-H^2\sinh x_3\kappa q\sinh\xi_3\kappa q\coth H\kappa q]/[\sinh^2 H\kappa q-(H\kappa q)^2] \\
&+(\delta_{j1}-\delta_{j3})\sum_{q=1}^{\infty}H(\kappa q)^2\cos\eta\kappa q[x_3\xi_3\cosh(x_3-\xi_3)\kappa q+H(x_3+\xi_3)\sinh\xi_3\kappa q\sinh x_3\kappa q \\
&-H\coth H\kappa q(x_3\sinh\xi_3\kappa q\cosh x_3\kappa q+\xi_3\sinh x_3\kappa q\cosh\xi_3\kappa q) \\
&+H^2\sinh x_3\kappa q\sinh\xi_3\kappa q/\sinh^2 H\kappa q]/[\sinh^2 H\kappa q-(H\kappa q)^2]\Big\},
\end{aligned}$$

$$j = 1, 2, 3, \quad \eta = x_1 - \xi_1, \quad \text{and} \quad \xi_3 < x_3. \tag{A 2}$$

For $x_3 < \xi_3$, replace x_3 by $H - x_3$, ξ_3 by $H - \xi_3$ and η by $-\eta$.

$$\begin{aligned}
D_{3,1}^{1,3} = \frac{\kappa}{2\pi\mu}\Big\{&(x_3-\xi_3)\sum_{q=1}^{\infty}\sin\eta\kappa q\sinh\xi_3\kappa q\sinh(H-x_3)\kappa q_3/\sinh H\kappa q \\
&+\sum_{q=1}^{\infty}\kappa q\sin\eta\kappa q[\pm x_3 H\sinh x_3\kappa q\sinh\xi_3\kappa q+\xi_3 x_3\kappa q H\sinh(x_3-\xi_3)\kappa q \\
&\pm x_3\xi_3\sinh H\kappa q\sinh(H-\xi_3-x_3)\kappa q\mp H(H-\xi_3)\sinh x_3\kappa q\sinh\xi_3\kappa q \\
&+H^2\kappa q(x_3\sinh\xi_3\kappa q\sinh(H-x_3)\kappa q \\
&-\xi_3\sinh x_3\kappa q\sinh(H-\xi_3)\kappa q)/\sinh H\kappa q]\,[\sinh^2 H\kappa q-(H\kappa q)^2]^{-1}\Big\}
\end{aligned}$$

$$\eta = x_1 - \xi_1, \quad \text{and} \quad \xi_3 < x_3. \tag{A 3}$$

The upper signs are to be used for D_3^1 and the lower signs for D_1^3. For $x_3 < \xi_3$ replace x_3 by $H - x_3$, ξ_3 by $H - \xi_3$, and η by $-\eta$. These expressions, although complicated looking, are easily calculable, all of them being decreasing exponential series. Techniques are similar to those given in LM.

REFERENCES

BLAKE, J. R. 1971 A note on the image system for a Stokeslet in a no-slip boundary. *Proc. Camb. Phil. Soc.* **70**, 303–310.

BLAKE, J. R. 1972 A model for the micro-structure in ciliated organisms. *J. Fluid Mech.* **55**, 1-23.

BLAKE, J. R. 1973 Flow in tubules due to ciliary activity. *Bull. Math. Biol.* **35**, 513–523.

BLAKE, J. R. & SLEIGH, M. A. 1974 Mechanics of ciliary locomotion. *Biol. Rev.* **49**, 85–125.

BLANDAU, R. J. 1969 Gamete transport – comparative aspects. In *The Mammalian Oviduct* (ed. E. S. E. Hafez & R. J. Blandau). University of Chicago Press.

BLUM, J. J. 1974 A note on fluid transport in ciliated tubules. *J. Theor. Biol.* **46**, 287–290.

LARDNER, T. J. & SHACK, W. J. 1972 Cilia transport. *Bull. Math. Biophys.* **34**, 325–335.

LIRON, N. 1976 On peristaltic flow and its efficiency. *Bull. Math. Biol.* **38**, 573–596.

LIRON, N. & MOCHON, S. 1976*a* Stokes flow for a Stokeslet between two parallel flat plates. *J. Engng Math.* **10**, 287–303.

LIRON, N. & MOCHON, S. 1976*b* The discrete-cilia approach to propulsion of ciliated microorganisms. *J. Fluid Mech.* **75**, 593–607.